Anal. Chem. **2002,** *74,* 5327−5332

Characterization of a Focal Plane Camera Fitted to a Mattauch−Herzog Geometry Mass Spectrograph. 1. Use with a Glow-Discharge Source

James H. Barnes IV,[†] Roger Sperline,[‡] M. Bonner Denton,[‡] Charles J. Barinaga,[§] David Koppenaal,[§] Erick T. Young,[⊥] and Gary M. Hieftje*[,†]

Department of Chemistry, Indiana University, Bloomington, Indiana 47405, Department of Chemistry, University of Arizona, Tucson, Arizona 85721, Pacific Northwest National Lab, Richland, Washington 99352, and Steward Observatory, University of Arizona, Tucson, Arizona 85721

A Mattauch−Herzog geometry mass spectrograph (MHMS) has been equipped with a novel array detector, the focal plane camera (FPC). The FPC consists of an array of gold Faraday cups, each coupled to its own integrator, with interrogation of the integrators performed by a multiplexer. The initial coupling of this instrument with a pin-type glow discharge source has provided limits of detection in the single to hundreds of nanograms per gram regime; isotope ratio accuracy and precision better than 5% error and 0.2% RSD, respectively; and a linear dynamic range of at least 6 orders of magnitude. A current weakness of the FPC is its pixel size, which limits both sensitivity and baseline resolution (to $R = 130$). The minimum data acquisition time for multiple images at present is 1 ms/image, with a dead time of 3.2 ms between images, which will limit the ability of the FPC to monitor extremely short transient signals.

Several types of mass spectrometers are capable of performing elemental analysis.[1] The major distinction between these types of instruments is in the way ions of differing masses are separated and detected. Quadrupole mass spectrometers (QMS) rapidly filter ions by scanning rf and dc potentials applied to the quadrupole rods.[2] These analyzers are popular because of their low cost, speed of analysis, and simplicity of operation. The major drawback, though, is that QMS instruments must scan to obtain a complete mass spectrum. This problem leads to spectral skew in transient signals and susceptibility to correlated noise, which can limit isotope ratio precision.

A type of mass analyzer that alleviates the need to scan a mass spectrum is the time-of-flight mass spectrometer (TOFMS).[3] In a TOFMS, ions are extracted simultaneously and accelerated into a field-free drift region with a uniform energy. The flight time is therefore proportional to the square root of the mass, so flight times can be converted to mass-to-charge (m/z) ratios to obtain a mass spectrum. These instruments overcome spectral skew and can reduce correlated (multiplicative) noise by ratioing, but they also have several limitations. Since TOFMS is inherently a pulsed technique, the duty cycle is poor: typically 10% or lower.[4] Additionally, the commercial instruments are currently more expensive than QMS instruments, mainly because of the sophisticated electronics needed for data acquisition and analysis.

A third type of commonly used mass analyzer is the sector field mass spectrometer (SFMS).[5,6] These instruments utilize an electrostatic analyzer to select a small range of ion energies and a magnetic field to disperse the ions spatially according to their m/z ratios. With the use of multiple detectors, simultaneous detection of a few m/z values is possible.[7] The high degree of spatial focusing available in SFMS instruments makes high-resolution measurements possible, permitting the separation of some isobaric overlaps, such as $^{40}Ar^{16}O^+$ from $^{56}Fe^+$.[8] Although simultaneous detection with such an instrument is possible, one cannot obtain a complete mass spectrum simultaneously with current commercially available SFMS instruments because of the presence of a curved focal plane and the limited number of detectors that can be positioned in the focusing region.

A type of SFMS geometry with a linear focal plane is the Mattauch−Herzog mass spectrograph (MHMS).[9] In this geometry, ion energies are focused by a 31.8° ($45° \times 2^{-1/2}$) electrostatic analyzer, which produces a collimated ion beam, followed by a magnetic sector, which deflects ions in the opposite direction by 90°. With a linear focal plane, an array detector can be used to detect all ions simultaneously. Simultaneous detection, as with a TOFMS, reduces multiplicative noise through ratioing. Additionally, duty cycle can be as high as 100%, a benefit that leads to reduced analysis time, less sample consumption, and improved detection limits.

* To whom correspondence should be addressed. Fax: 1-812-855-0958. E-mail: hieftje@indiana.edu.

[†] Indiana University.

[‡] Department of Chemistry, University of Arizona.

[§] Pacific Northwest National Lab.

[⊥] Steward Observatory.

(1) Bacon, J. R.; Crain, J. S.; Van Vaeck, L.; Williams, J. G. *J. Anal. At. Spectrom.* **2001**, *16*, 879−915.

(2) Miller, P. E.; Denton, M. B. *J. Chem. Educ.* **1986**, *63*, 617−622.

(3) Wiley, W. C.; McLaren, I. H. *Rev. Sci. Instrum.* **1955**, *26*, 1150−1157.

(4) Dawson, J. H. J.; Guilhaus, M. *Rapid Commun. Mass Spectrom.* **1989**, *3*, 155−159.

(5) Jakubowski, N.; Moens, L.; Vanhaecke, F. *Spectrochim. Acta, Part B* **1998**, *53B*, 1739−1763.

(6) Becker, J. S.; Dietze, H.-J. *Spectrochim. Acta, Part B* **1998**, *53B*, 1475−1506.

(7) Halliday, A. N.; Lee, D.-C.; Christensen, J. N.; Walder, A. J.; Freedman, P. A.; Jones, C. E.; Hall, C. M.; Yi, W.; Teagle, D. *Int. J. Mass Spectrom. Ion Processes* **1995**, *146/147*, 21−33.

(8) Jakubowski, N.; Feldmann, I.; Stuewer, D. *J. Anal. At. Spectrom.* **1997**, *12*, 151−157.

(9) Mattauch, J.; Herzog, R. *Z. Phys.* **1934**, *89*, 786−795.

10.1021/ac020304z CCC: $22.00
Published on Web 09/07/2002

The two main types of array detectors used for most mass spectrometric applications are photographic emulsions[10,11] and electrooptical imaging detectors (EOID).[12,13] Photographic emulsions are time-consuming to prepare and even with significant care in calibration, plate-to-plate variations limit the accuracy of quantification. The EOID consists of a microchannel plate amplifier (MCP), which converts ions to electrons, followed by a phosphor screen or scintillating crystal to convert the electrons to photons, which are then detected with an array detector, such as a photodiode array or CCD camera. An EOID is limited in resolution by the pore size of the MCP and by the fidelity of focusing of electrons that traverse the gap between the MCP and the photoemitter. Moreover, relatively high background noise limits the performance of the EOID. In both of these detection systems, the dynamic range is limited by the most intense peak incident on the array detector. Because of these problems, a better array detector for mass spectrometric analysis is needed.

At present, several new array detectors for mass spectrometry are in various stages of development.[14−20] One of these array detectors, termed a focal plane camera (FPC), has been developed by Knight et al.[21] This novel device combines an array of Faraday cups, each with its own low-capacitance integrator, with a multiplexed readout. This detector has several advantages over conventional mass spectrometric array detectors. Unlike photographic plates or the EOID, the FPC directly converts ions into an electronic signal, reducing the level of noise introduced in the data-acquisition process. Additionally, the signal from the Faraday cups is integrated directly and continuously, and each integrator can be interrogated nondestructively, a benefit that leads to an improved signal-to-noise ratio. Finally, the dynamic range is not limited by the most intense m/z ratio.

The present work characterizes the FPC as an array detector for a glow discharge ionization source Mattauch−Herzog geometry mass spectrograph. Figures of merit, including limits of detection, isotope ratio precision and accuracy, resolution, and dynamic range are presented. Additionally, the ability to monitor transient signals was tested by using a millisecond-pulsed glow discharge ionization source.

EXPERIMENTAL SECTION

Instrumentation. An in-house-built Mattauch−Herzog geometry mass spectrograph (MHMS) was used in all experimentation and has been described elsewhere.[22−24] In previous studies, the MHMS has been equipped with several ionization sources, including an inductively coupled plasma (ICP),[23] both pulsed and dc glow discharges (GD),[22,25] and a microwave plasma torch (MPT). In the present study, a pin-type glow discharge source was used because it is well-characterized, simple to operate, and less prone to noise than either the ICP or MPT. In this geometry, the sample serves as the cathode and the skimmer cone of the mass-spectrometer interface as the anode. Moreover, the pin-type geometry permits simple sample positioning and changing. Argon (Air Products, Allentown, PA, 99.998%) was supplied to the GD source by a mass flow controller (MKS 1179A, Andover, MD) and digital controller unit (MKS 247A). In dc operation, the GD source was powered by a Kepco power supply (BHK 1000−0.2M, New York City), whereas in pulsed operation, the source was powered by an IRCO power supply (M3k-20-N, Columbia, MD).

Ions are extracted from the GD source through a differentially pumped interface that includes a skimmer (0.9-mm aperture diameter) and a third-stage aperture (1.0-mm aperture diameter). A 1.00 kV potential is applied between the skimmer and the third stage aperture to accelerate the ion beam into the mass analyzer portion of the instrument. Once in the third stage, the ion beam is shaped and focused onto a slit (100-μm width) by means of an Einzel lens and a dc quadrupole doublet. An electrostatic analyzer (ESA) is used to compensate for the energy spread in the slit-shaped ion beam. In the Mattauch−Herzog geometry, the ion beam is collimated as it leaves the ESA and enters the magnetic sector. Ions are deflected by 90° in the magnetic sector and dispersed and focused along a plane in accordance with their m/z ratios. The potentials applied to the Einzel lens, quadrupole doublet, and ESA are varied in order to maximize signal level as well as to improve peak shape and resolution.

Metal Standards. For LOD, resolution, and dynamic range determinations, as well as in the pulsed GD studies, a 0.25-in. (6.4 mm)-diameter stainless steel pin (NIST SRM 443, Gaithersburg, MD) was used as the cathode. This sample contained elemental concentrations from 0.0008% Ta to 68.0% Fe. For the isotope ratio accuracy and precision measurements, a 0.25-in. (6.4 mm)-diameter pin of titanium (6V 4AL aircraft grade, Halpern Titanium, Three Rivers, MA) was used. This sample was substituted because the NIST sample did not contain any element of appreciable concentration with two isotopes of roughly equal abundance that were in a region of the mass spectrum free of isobaric interferences and that could be resolved with the current detector. Because quantitative concentration information was not the concern of this study, a certified concentration value is unnecessary. Moreover, the natural abundance of titanium isotopes does not fluctuate to a high degree, regardless of the source, because of the low number of radioisotopes with decay pathways that lead to titanium.

Focal Plane Camera. The FPC was developed at the University of Arizona by Knight et al.[21] in conjunction with Spectral Instruments (Tucson, AZ). In this study, 31 of the Faraday cup pixels were utilized for data acquisition. The pixels were spaced

(10) Guthrie, J. W.; Repetti, A. A. *Rev. Sci. Instrum.* **1966**, *37*, 1425−1426.
(11) McCrea, J. M. *Appl. Spectrosc.* **1967**, *21*, 305−311.
(12) Giffin, C. E.; Boettger, H. G.; Norris, D. D. *Int. J. Mass Spectrom. Ion Phys.* **1974**, *15*, 437−449.
(13) Boettger, H. G.; Giffin, C. E.; Norris, D. D.; Dreyer, W. J.; Kuppermann, A. *Adv. Mass Spectrom. Biochem. Med.* **1977**, *2*, 513−524.
(14) Langstaff, D. P. *Int. J. Mass Spectrom.* **2002**, *215*, 1−12.
(15) Selby, D. S.; Mlynski, V.; Guilhaus, M. *Int. J. Mass Spectrom.* **2002**, *215*, 31−43.
(16) Kraus, H. *Int. J. Mass Spectrom.* **2002**, *215*, 45−58.
(17) Nevejans, D.; Neefs, E.; Kavadias, S.; Merken, P.; Van Hoof, C. *Int. J. Mass Spectrom.* **2002**, *215*, 77−87.
(18) Berthelier, J.-J.; Illiano, J.-M.; Nevejans, D.; Neefs, E.; Arijs, E.; Schoon, N. *Int. J. Mass Spectrom.* **2002**, *215*, 89−100.
(19) Fuerstenau, S.; Soli, G.; Cunningham, T.; Hancock, B.; Pain, B.; Sinha, M. *Int. J. Mass Spectrom.* **2002**, *215*, 101−111.
(20) Birkinshaw, K. *Int. J. Mass Spectrom.* **2002**, *215*, 195−209.
(21) Knight, A. K.; Sperline, R. P.; Hieftje, G. M.; Young, E.; Barinaga, C. J.; Koppenaal, D. W.; Denton, M. B. *Int. J. Mass Spectrom.* **2002**, *215*, 131−139.
(22) Solyom, D. A.; Burgoyne, T. W.; Hieftje, G. M. *J. Anal. At. Spectrom.* **1999**, *14*, 1101−1110.
(23) Solyom, D. A.; Gron, O. A.; Barnes, J. H. I.; Hieftje, G. M. *Spectrochim. Acta, Part B* **2001**, *56*, 1717−1729.
(24) Burgoyne, T. W.; Hieftje, G. M.; Hites, R. A. *J. Am. Soc. Mass Spectrom.* **1997**, *8*, 307−318.
(25) Solyom, D. A.; Hieftje, G. M. *J. Anal. At. Spectrom.* **2002**, *17*, 329−333.

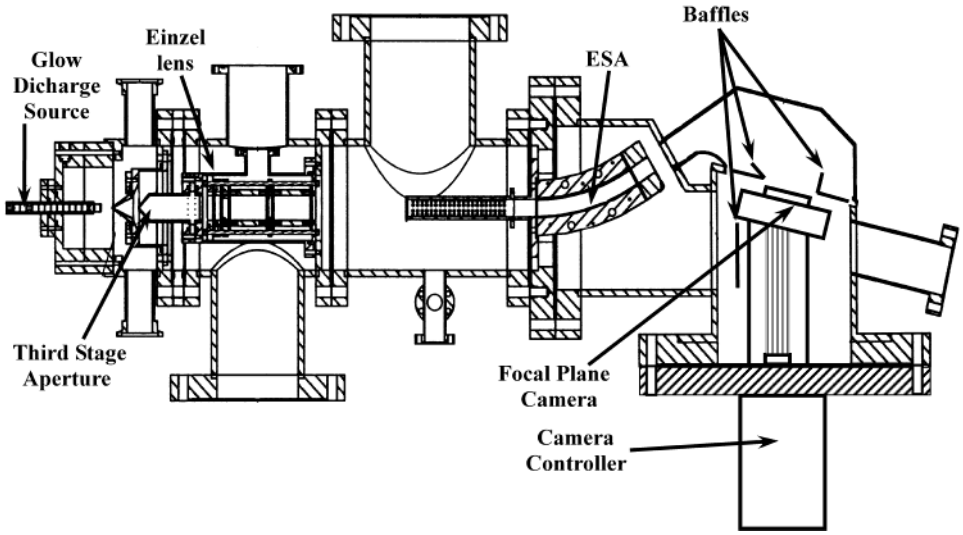

Figure 1. Aluminum baffle locations used to block stray ions from striking the FPC.

Table 1. Operating Conditions of the GD-MHMS-FPC

glow discharge source	
discharge voltage	1000 V
discharge current	15−50 mA
discharge pressure	0.5−0.9 Torr
sampling distance	0.5−1.5 cm
mass spectrograph	
entrance slit width	100 μm
skimmer aperture	0.9 mm
third-stage aperture	1.0 mm
second-stage pressure	$(1-2) \times 10^{-4}$ Torr
third-stage pressure	$(1-3) \times 10^{-6}$ Torr
accelerating potential	1000 V
ion optic potentials	variable
magnet field strength	1000−10 000 G
focal plane camera	
Faraday cup width	145 μm
Faraday cup height	1.6 mm
pixel spacing on center	175 μm
active pixels	31
FPC backplate temperature	−40°

175 μm on center and separated by 10-μm-wide ground wires with 10-μm spacing between the pixels and ground wires. The camera was refrigerated to −40°C by a Peltier cooler. Integration time can be varied between 1 ms and 20 s, with either destructive or nondestructive readout mode data acquisition. The camera was mounted at an angle of 13.2° with respect to its Conflat flange mounting on four spring-loaded supports to match the angle of the focal plane. Additionally, it was positioned at the center of the focal plane, corresponding to a radius of curvature of 72.7 mm for the innermost pixel and 78.1 mm for the outermost pixel. Because the present pixel array covers only a small portion of the focal plane, the magnetic field strength was varied to move the desired m/z range onto the array. The important operating parameters associated with the glow discharge source, MHMS, and FPC are detailed in Table 1.

RESULTS AND DISCUSSION

Detector Shielding. It was observed that when high ion fluxes are incident upon the unconnected pixels or the circuit-board portion of the camera, large negative signals are obtained. A possible cause of these problems could be localized voltages, which arise from intense ion fluxes at specific m/z ratios ($^{40}Ar^+$ and $^{56}Fe^+$) that adversely affect the exposed camera electronics. To minimize this problem, small sheets of 1/16 in (1.6 mm) aluminum were installed as baffles to block the portion of the ion beam not incident on the active portion of the camera, as shown in Figure 1. Two baffles were placed ∼1 mm inside the magnetic sector on both sides of the active pixels. An additional baffle was placed on the ionization-source side of the camera support to block stray ions from affecting the controlling electronics along the backside of the pixel array. The baffles dramatically reduced the negative signals observed with the camera.

As described by Knight et al.,[21] the Faraday cups were designed to differ in length across the array in order to test the effects of the length on the capacitance and subsequently the read noise. This design, of course, provides differing active pixel areas across the array. Since the incident ion flux is distributed evenly over the height of the focal plane, the collection ability of a Faraday cup is proportional to its surface area, and therefore, the differing pixel sizes caused a pixel-dependent response across the array. To eliminate this nonuniform response, a copper shield was placed ∼0.5 mm above the pixels and across two-thirds of the height of the array. The shield made the effective size of all the Faraday cups one-third height, or ∼1.6 mm high. Of course, in later detector designs, it will be possible to make the Faraday plates longer to match the height of the mass spectrometer flight tube, which in the present case is 6.4 mm. A factor of 4 higher sensitivity could be realized.

Limits of Detection. Ion signals for limit-of-detection calculations were accumulated for 10 10-s integrations with a NIST 443 stainless steel sample. In cases in which the ion signal was too large to be integrated for 10 s, several shorter integration periods were summed to obtain the desired integration period. Equation 1 was used to calculate detection limits.[26]

$$\mathrm{DL}_x = [X]\left(\frac{3\sigma}{A}\right)n^{1/2} \qquad (1)$$

In eq 1, X is the concentration of the analyte of interest; σ is the

(26) Brushwyler, K. R.; Furuta, N.; Hieftje, G. M. *Talanta* **1990**, *37*, 23−32.

Table 2. Limits of Detection, parts per billion, Corrected for Isotopic Abundance, for Various Elements Using the FPC[a], an Electron Multiplier[b], and the EOID[c]

	LOD		
isotope	FPC	electron multiplier	EOID
Ti 49	5	60	
V 51	25		
Cr 53	301		
Mn 55	126		
Co 59	109		
Ni 62	133		
Cu 63	853		
Nb 93	19		
Mo 100	48	20	3000
Sn 124	36	10	
Ta 181	17	4	
W 180	21	5	20000
Pb 204		3	25000
Pb Total	269		

[a] Focal plane camera, new in this study. [b] Values taken from ref 18. [c] Electrooptic imaging detector; values taken from ref 20.

standard deviation of the blank, in this case the dark current of the pixels with the accelerating potential off; A is the integrated signal, and n is the number of points used to calculate σ and A. Limits of detection corrected for isotopic abundance for a range of elements are listed in Table 2. The LOD range extends from single nanograms per gram (parts-per-billion) (5 for ^{49}Ti) to hundreds of nanograms per gram (853 for ^{63}Cu), with most elements in the tens of nanograms per gram regime. Additionally, Table 2 compares these values to previous LODs obtained with the GD-MHMS in scanning mode with an electron multiplier detector and in simultaneous mode with an earlier array detector, the electrooptical imaging detector (EOID). The FPC give LOD values within an order of magnitude of those from the electron multiplier, and nearly 3 orders of magnitude better than those with the EOID. It should be noted that the area of each of the FPC pixels in this study is approximately a factor of 4 smaller than the exit slit area used in the electron multiplier study. When this geometric factor is considered, the results of the two studies are comparable.

Isotopic Ratio Accuracy and Precision. Isotopic ratio accuracy and precision were determined using 10 integration periods for the isotopes of titanium. Titanium was chosen because four of its five isotopes are of roughly equal concentration and located in a region of the mass spectrum that is relatively free of isobaric interferences. The determined error in accuracy is <5% for all isotopic ratios, averages 1−3%, and is not improved by integration times longer than 0.2 s, as shown in Figure 2. The only exception is for ratios involving ^{50}Ti, which suffer greater error as a result of the high levels of vanadium and chromium in the sample and their isobaric overlap with ^{50}Ti. These values are similar to those obtained with an electron multiplier in scanning mode (1−3% error for W isotopes[25]) and slightly better than simultaneous detection with the EOID (4% error for Pb isotopes[27]).

The ^{46}Ti/^{47}Ti and ^{49}Ti/^{50}Ti isotope ratio precision improved roughly as the square root of integration time, as shown by the log−log plot in Figure 3. This behavior suggests that precision is limited by counting statistics. This plot did not deviate from

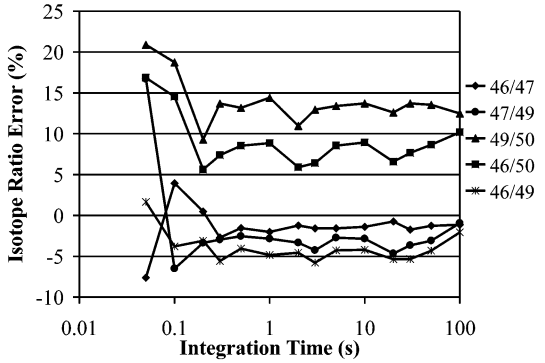

Figure 2. Isotope ratio accuracy for the isotopes of titanium.

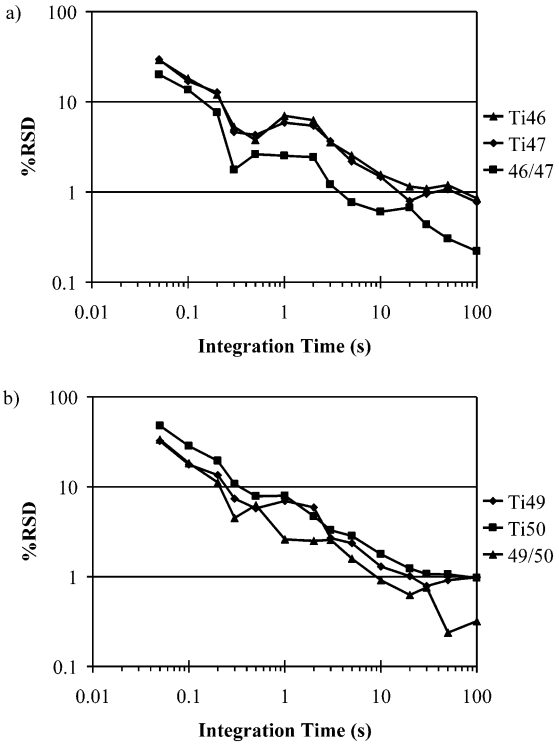

Figure 3. Effect of integration time on isotope ratio precision for (a) ^{46}Ti and ^{47}Ti and (b) ^{49}Ti and ^{50}Ti.

linearity through integration times above 100 s/image. Data were not collected at longer integration times because of present limitations of the data acquisition software. With integration times of this length, the isotope ratio precision was 0.2%. It should be noted that the ratio precision is slightly better than the precision of each isotope, indicating the presence of some correlated noise. These values are slightly better than those obtainable with an electron multiplier (0.3% RSD for W isotopes[25]) or EOID (0.5% RSD for Pb isotopes[27]). Presumably, precision should improve even more with longer integration times once new software becomes available.

Resolution. In the MHMS geometry, the peak width remains constant throughout the mass spectrum to a good approximation, whereas the peak spacing decreases in proportion to the square root of the m/z ratio. Therefore, as the m/z ratio goes up, the peak spacing will lessen until peaks are located on every pixel. To confidently distinguish between two consecutive m/z ratios, one must have at least one pixel between each pair of peaks. This property of the MHMS limits complete resolution of consecutive

(27) Solyom, D. A., Ph. D. thesis, Indiana University, Bloomington, 2001.

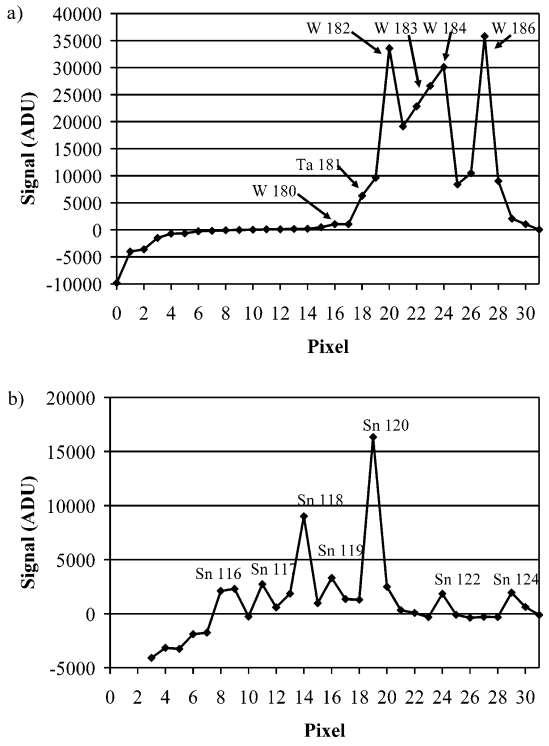

Figure 4. Resolving power of the GD-MHMS-FPC is limited by pixel spacing on the present camera. (a) Tungsten isotopes cannot be individually distinguished; (b) tin isotopes can be resolved, even with uneven peak spacing inherent in the Mattauch−Herzog geometry.

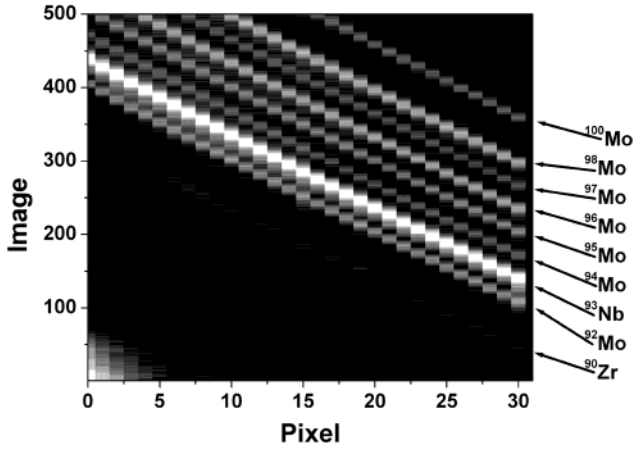

Figure 5. Contour map covering a range of $m/z = 90-100$. The periodicity observed is due to the 30-μm space between each pair of Faraday cups.

m/z ratios to below 190 with the current operating conditions, as shown in Figure 4a. Additionally, because of the nonuniform peak spacing, the ability to resolve a range of m/z ratios requires the peaks to be separated by more than one pixel, which limits the highest resolvable m/z to ~130 and below, as shown in Figure 4b.

The MHMS was operated in scanning mode to verify that pixel size was the limiting factor in the resolution. With 31 detector elements, operating in this mode is analogous to using 31 single-channel detectors. During previous scanning-mode studies with the MHMS, an exit slit was place along the focal plane. In this study, the physical spacing of the pixels provides adequate exit slits, each 145 μm wide. Figure 5 shows a contour map of the

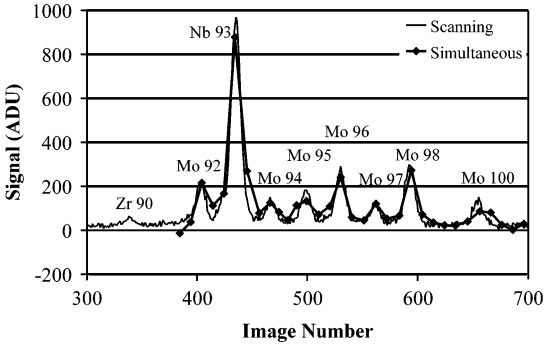

Figure 6. Mass spectra obtained in both simultaneous and scanning mode detection.

zirconium, molybdenum, and niobium isotopes obtained by scanning the magnetic field strength. Molybdenum and niobium are certified as 0.12 and 0.06%, respectively, whereas the source of zirconium is the insulator used to shield the cathode from the glow discharge cell. Along the pixel axis, a simultaneous mass spectrum is obtained, but along the image axis, a scanning mass spectrum is obtained. When the two detection axes are compared, as in Figure 6, the pixel size limitation becomes apparent. Resolving power (fwhm) is improved to 300 by scanning. This value is approximately a factor of 2 poorer than the theoretical resolving power on the basis of a 145-μm slit width but is a factor of 2 better than that obtainable in simultaneous acquisition mode.

To increase the physical spacing of adjacent m/z values, one could lower the accelerating potential and magnetic field strength, but at a cost to operating performance. As the accelerating potential declines, the sensitivity drops dramatically as a result of space charge effects. Because of these adverse effects, the accelerating potential was not lowered, and the resolving power is presently limited to 190. In previous studies, the resolving power of the MHMS has been reported to be as high as 800 with an electron multiplier and scanning-mode operation[25] and 490 with the EOID and simultaneous detection.[27] This figure of merit is one that will improve dramatically with future generations of the camera in which the pixel width is narrower.

Dynamic Range. The FPC should provide a dynamic range of 8 orders of magnitude when one considers the linearity of the analog-to-digital converter (1 to 10 000) and the selectable range of integration times (1 ms to 20 s). For the present study, no available solid sample series had a concentration range of 10 orders of magnitude for a given element. As a rough approximation of this range, though, the NIST 443 sample can be used. It contains multielemental concentrations ranging from 0.000 17% for ^{49}Ti to 62.3% for ^{56}Fe, a range that covers almost 6 orders of magnitude. Although there is a slightly different instrumental response for each element, the plot in Figure 7 shows a good degree of linearity, as indicated by the $R^2 = 0.949$. Deviations from linearity can best be attributed to the nonideal nature of the experiment.

Pulsed Glow Discharge. A millisecond pulsed GD was used to test the ability of the FPC to record transient signals. The glow-discharge power supply was operated with the longest pulse width possible (10 ms) and at a low repetition frequency (1.3 Hz). Figure 8 shows the detector response for $^{56}Fe^+$ with a 1-ms integration time/image and no nondestructive readouts. On the basis of the

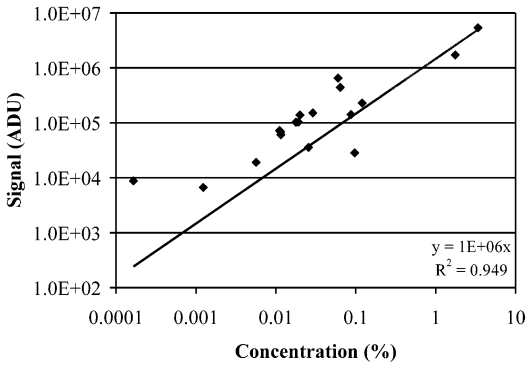

Figure 7. Dynamic range of the GD-MHMS-FPC, showing 6 orders of magnitude linear range. In the present study, this range was limited by concentrations in the available samples. Further, scatter in this plot is the result of several elements having different sensitivities (but also different concentration ranges being utilized).

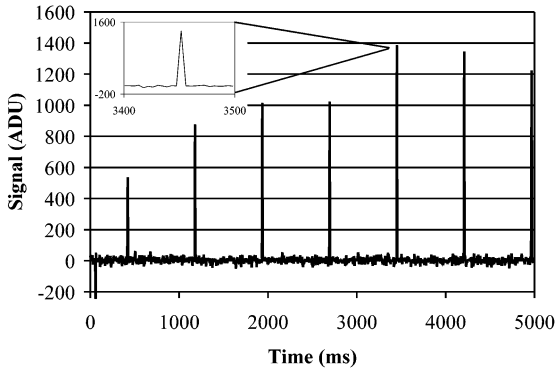

Figure 8. ^{56}Fe peaks produced by a 10-ms pulsed glow discharge operating at a repetition frequency of 1.3 Hz.

frequency of operation and the number of images between pulses, one can calculate a total acquisition time of 4.2 ms/image, corresponding to dead time of 3.2 ms between two integration periods. To accurately map out a peak, one would desire a minimum of 5−10 data points, a value that corresponds to a minimum time of 40−80 ms/transient event.

CONCLUSIONS

The FPC shows a great deal of promise. Although it is at an early stage in its development, the figures of merit are already comparable to those of a well-established single-channel detector, the electron multiplier, and are orders of magnitude better than those of a comparable array detector, the EOID. Limits of detection fall in the tens of ppb regime. Isotope ratio accuracy and precision are below 5% error and 0.2% RSD, respectively. The dynamic range of the FPC is at least 6 orders of magnitude. Currently, there are two main weaknesses to the camera. The first is pixel size, which limits the ability to resolve high m/z ratio ions and also limits the height of an incoming ion beam that can be intercepted. The second is the adverse effect of intense ion fluxes on the response of the detector. The former will be solved in future generations of the camera by adjusting the pixel size and number, whereas the latter will be improved by better physical detector shielding.

ACKNOWLEDGMENT

Support for this work was provided by the U.S. Department of Energy, Office of Nonproliferation Research and Engineering. Pacific Northwest National Laboratory is operated by Battelle Memorial Institute for the Department of Energy under contract DE-AC06-76RLO-1830.

Received for review May 7, 2002. Accepted July 27, 2002.

AC020304Z